Molecular Cancer Research

CD38 Inhibits Prostate Cancer Metabolism and Proliferation by Reducing Cellular NAD$^+$ Pools

Jeffrey P. Chmielewski[1], Sarah C. Bowlby[1], Frances B. Wheeler[1], Lihong Shi[1], Guangchao Sui[1], Amanda L. Davis[1], Timothy D. Howard[2], Ralph B. D'Agostino Jr[3,4], Lance D. Miller[1,3], S. Joseph Sirintrapun[5], Scott D. Cramer[6], and Steven J. Kridel[1,3]

Abstract

Tumor cells require increased rates of cell metabolism to generate the macromolecules necessary to sustain proliferation. They rely heavily on NAD$^+$ as a cofactor for multiple metabolic enzymes in anabolic and catabolic reactions. NAD$^+$ also serves as a substrate for PARPs, sirtuins, and cyclic ADP-ribose synthases. Dysregulation of the cyclic ADP-ribose synthase CD38, the main NAD'ase in cells, is reported in multiple cancer types. This study demonstrates a novel connection between CD38, modulation of NAD$^+$, and tumor cell metabolism in prostate cancer. CD38 expression inversely correlates with prostate cancer progression. Expressing CD38 in prostate cancer cells lowered intracellular NAD$^+$, resulting in cell-cycle arrest and expression of p21^{Cip1} (CDKNA1). In parallel, CD38 diminishes glycolytic and mitochondrial metabolism, activates AMP-activated protein kinase (AMPK), and inhibits fatty acid and lipid synthesis. Pharmacologic inhibition of nicotinamide phosphoribosyltransferase (NAMPT) mimicked the metabolic consequences of CD38 expression, demonstrating similarity between CD38 expression and NAMPT inhibition. Modulation of NAD$^+$ by CD38 also induces significant differential expression of the transcriptome, producing a gene expression signature indicative of a nonproliferative phenotype. Altogether, in the context of prostate cancer, the data establish a novel role for the CD38–NAD$^+$ axis in the regulation of cell metabolism and development.

Implications: This research establishes a mechanistic connection between CD38 and metabolic control. It also provides the foundation for the translation of agents that modulate NAD$^+$ levels in cancer cells as therapeutics. *Mol Cancer Res; 16(11); 1687–700. ©2018 AACR.*

Introduction

NAD$^+$ metabolism is associated with everything from aging and healthy lifespan, to diabetes, neurocognitive function, and cancer, among others (1, 2). NAD$^+$ connects to cellular metabolism in various ways. First, it is a necessary cofactor for multiple anabolic and catabolic reactions, in doing so providing a crucial link to energy production and macromolecular synthesis (3). For example, NAD$^+$ is reduced to NADH during glycolysis and the tricarboxylic acid (TCA) cycle, producing an electron carrier for subsequent ATP generation. Conversely, the phosphorylated form, NADPH, is a cofactor for fatty acid synthesis. Because deregulated cellular metabolism is an established hallmark of oncogenic transformation, it is reasonable to assume NAD$^+$ metabolism must be regulated accordingly (4).

There are multiple pathways by which NAD$^+$ can be synthesized, and they can be segregated into either the *de novo* or salvage pathways. Most tissues and oncogenic cells synthesize NAD$^+$ via the salvage pathway (5). The salvage pathway is a two-step reaction that recycles nicotinamide into NAD$^+$ and is catalyzed by nicotinamide phosphoribosyltransferase (NAMPT). NAD$^+$ turnover in cancer cells is dramatically increased relative to nonproliferating healthy cells, making NAD$^+$ metabolism an attractive therapeutic target (6). NAD$^+$ levels can also be modulated by enzymatic consumption. There are three classes of enzymes that consume NAD$^+$: the PARPs, sirtuins, and cyclic ADP-ribose (ADPR) synthases (7–9). Although PARPs and sirtuins have multiple roles in cancer biology, including response to DNA-damaging reagents and modulation of protein modification, among others, CD38 is the primary NAD'ase in mammalian cells (10). CD38 is a cyclic ADPR synthase that localizes to the cell membrane and elsewhere throughout the cell including the endoplasmic reticulum (ER), Golgi, and mitochondria (11, 12). CD38 hydrolyzes NAD$^+$ to produce ADPR, which is covalently attached to proteins to modify their function (9). Alterations in CD38 expression occur in a variety of cancers including hematologic malignancies, glioma, pancreatic cancer, and prostate cancer (13–15). Decreased expression of CD38 in prostate luminal cells is sufficient to drive prostate cancer and is linked to lower overall survival (16). Conversely, *CD38* expression is higher in pancreatic cancer compared with normal tissue (17). Although expression of CD38 is linked to disease progression, the metabolic consequences of CD38 expression in prostate cancer have not been defined.

[1]Department of Cancer Biology, Wake Forest School of Medicine, Winston-Salem, North Carolina. [2]Department of Biochemistry, Wake Forest School of Medicine, Winston-Salem, North Carolina. [3]Comprehensive Cancer Center at Wake Forest Baptist Medical Center, Winston-Salem, North Carolina. [4]Public Health Sciences-Department of Biostatistical Sciences, Wake Forest School of Medicine, Winston-Salem, North Carolina. [5]Department of Pathology, Memorial Sloan Kettering Cancer Center, New York, New York. [6]Department of Pharmacology, University of Colorado Denver, Aurora, Colorado.

Corresponding Author: Steven J. Kridel, Wake Forest University Health Sciences, Medical Center Blvd., Winston-Salem, NC 27157. Phone: 336-716-7299; Fax: 336-716-0255; E-mail: skridel@wakehealth.edu

doi: 10.1158/1541-7786.MCR-17-0526

©2018 American Association for Cancer Research.

Downloaded from http://aacrjournals.org/mcr/article-pdf/16/11/1687/2312911/1687.pdf by guest on 27 August 2022

We previously demonstrated that NAMPT activity is required to support fatty acid and lipid synthesis in prostate cancer (18). Therefore, we hypothesized that CD38, through its NAD'ase activity, also regulates energy production and lipid synthesis in prostate cancer. The data presented herein demonstrate that CD38 expression is reduced in prostate cancer and that expressing CD38 in prostate cancer cells affects multiple metabolic processes to reprogram cells in favor of a nonproliferative state. Collectively, our data suggest that loss of CD38 is a key event in oncogenic transformation in prostate that confers a metabolic advantage to tumor cells, thus providing new insight into the mechanisms underlying tumor cell metabolism.

Materials and Methods

Materials

Antibodies for acetyl-CoA carboxylase 1 (ACC1), phospho-ACC1 (S79), AMPK, phospho-AMPK (T172), Sirt1, and Sirt3 (C73E3) were obtained from Cell Signaling Technology, antibodies against CD38 and FOXO1 were from Abcam, antibodies for SLC22A3 and β-actin were purchased from Sigma-Aldrich, and antibody for Ac-FOXO1 was purchased from Santa Cruz Biotechnology, Inc. Secondary antibodies for goat anti-mouse and goat anti-rabbit were purchased from Bio-Rad. The NAMPT inhibitor FK866 was obtained from Cayman Chemical Company. NAD^+, nicotinamide mononucleotide (NMN), doxycycline hyclate, and puromycin dihydrochloride were purchased from Sigma-Aldrich. ^{14}C-Acetate was purchased from PerkinElmer and ^{14}C-choline from American Radiolabeled Chemicals. Retinoic acid (all-*trans*-retinoic acid; ATRA) and 5-azacytidine (Aza) were obtained from Sigma-Aldrich. All primers for qPCR were purchased from Integrated DNA Technologies.

Cell culture, drug treatments, and transfection

LNCaP, PC-3, and DU145 cell lines were obtained from the ATCC. Normal prostate epithelial cells (PREC) were obtained from Lonza. Cells were routinely subjected to *Mycoplasma* testing. Prostate cancer cell lines were cultured in RPMI1640 (Gibco) supplemented with 10% FBS, penicillin (100 U/mL), and streptomycin (100 μg/mL) at 37°C and 5% CO_2. PRECs were cultured in Clonetics prostate cell growth medium as directed by the manufacturer. Cell lines and clones were used over 10 to 20 passages following thawing. FK866 was dissolved in DMSO and used at the concentrations and times as indicated. Vehicle control cells were treated with DMSO (0.01%). NMN (500 μmol/L) and NAD^+ (100 μmol/L) were dissolved in sterile water and cotreated with FK866 at the time of administration.

For transfection, cells were cultured in RPMI1640 and 10% FBS without antibiotics for 48 hours prior to seeding. After seeding, cells were transfected with varying amounts (500 ng–2 μg) of plasmid DNA containing either the *CD38* cDNA under the direction of a doxycycline-inducible promoter or the same vector without *CD38*. Cells were transfected using Lipofectamine LTX with Plus Reagent (Thermo Fisher Scientific). Transfected cells were selected with puromycin (4 μg/mL; Sigma-Aldrich) until individual colonies were formed. Clonal populations were established from single colonies and maintained on puromycin (1 μg/mL) to retain selection, and CD38 was induced with doxycycline (1 μg/mL) for the indicated times.

IHC of CD38 expression

CD38 staining intensity was determined from benign, prostatic intraepithelial neoplasia (PIN), and prostate adenocarcinoma cores from a tissue microarray obtained from BioMax Inc. Slides were deparaffinized and rehydrated by xylene/ethanol wash. Slides were then incubated with antigen unmasking solution in a pressure cooker at 97°C for 30 minutes. Cooled slides were blocked in 1% BSA in 1× PBS for 10 minutes at room temperature. CD38 antibody was incubated at a 1:1,000 dilution in 1% BSA overnight at 4°C. Slides were washed three times with PBS and incubated with horseradish peroxidase secondary antibodies, incubated for 10 minutes in 3, 3-diaminobenzidine (DAB) solution, washed three times in 1× PBS, and counterstained with hematoxylin. TMA cores were independently scored by staining intensity ranging from 0 to 3, with 0 representing the lowest intensity.

Western blotting

Cells were treated as indicated for individual experiments, harvested, washed with 1× cold PBS, and lysed in buffer containing 1% Triton X-100, 20 mmol/L Tris-HCl (pH 8.3), 5 mmol/L EDTA, and protease inhibitors (1 μmol/L sodium orthovanadate, 1 μmol/L sodium fluoride, 200 nmol/L okadaic acid, 5 μg/mL aprotinin, pepstatin, and leupeptin, and 200 μmol/L PMSF). Protein concentrations for individual samples were assayed using Bio-Rad DC reagents, using BSA as a standard. Samples were resolved via SDS-PAGE and transferred to nitrocellulose blotting membrane. Membranes were blocked and incubated with primary and secondary antibodies as described previously (18). Enhanced chemiluminescence (PerkinElmer Life Sciences) was used to detect immunoreactive bands.

Total NAD^+ quantification

Quantification of total cellular NAD^+ was performed using an EnzyChrom NAD^+/NADH Assay Kit as described previously (18). Briefly, cells were seeded (1.5×10^5 cells/dish) in triplicate in 10-cm dishes and treated as indicated. After treatment, cells were harvested by trypsinization, counted, and NAD^+ determined according to the manufacturer's instructions. Total NAD^+ levels were normalized to protein from an equivalent number of cells and made relative to vehicle-treated cells.

Cell count and viability assays

Prostate cancer cells were plated in 6-well plates in triplicate and allowed to adhere for 24 hours prior to treatment with doxycycline (1 μg/mL) or ATRA. At the indicated time points, cells were trypsinized, pelleted, and resuspended in a known volume. Cell counts were established using a Countess automated cell counter. Live versus dead cells were quantified by trypan blue exclusion using a Countess automated cell counter. Cell growth was determined by normalizing cell numbers at the indicated time points to the number of cells plated. Doubling times were determined using relative growth values from T24 and T96 time points.

The viability of cells expressing CD38 treated with FK866 was determined using CellTiter-Glo 2.0 (Promega). Briefly, cells treated with vehicle or doxycycline (1 μg/mL) were plated in 96-well plates ($n = 7$) and allowed to adhere for 8 hours prior to the addition of FK866. Luminescence was detected using a FLUOstar Optima spectrometer (BMG Labtech), and viability was determined relative to control.

Downloaded from http://aacrjournals.org/mcr/article-pdf/16/11/1687/2312911/1687.pdf by guest on 27 August 2022

Cell-cycle analysis

Prostate cancer cells were treated with doxycycline (1 μg/mL) or vehicle for 96 hours. They were then trypsinized, washed twice in cold PBS, and fixed in cold 70% methanol for 30 minutes at 4°C. Following fixation, cells were washed twice with PBS and treated with RNase A (100 μg/mL) for 15 minutes (Thermo Fisher Scientific) followed by staining with propidium iodide (50 μg/mL; Invitrogen). Flow cytometry was performed on a Becton Dickinson Accuri C6 analyzer and analyzed using FlowJo V10 software (FlowJo, LLC.). The percent of cells in each phase of the cell cycle was determined using the Watson Pragmatic algorithm available in the FlowJo software.

Determination of *CD38* gene methylation status

Prostate cancer cells were seeded in 10-cm dishes and allowed to adhere overnight before treating with ATRA (1.2 μmol/L) or azacytidine (5 μmol/L) for 96 hours. They were then trypsinized, washed twice with PBS, and lysed in Qiagen Buffer RLT buffer supplemented with 2-mercaptoethanol (140 μmol/L; Sigma-Aldrich). DNA/RNA purification was performed using an AllPrep DNA/RNA Mini Kit (Qiagen). Pyrosequencing assays were designed using PyroMark Assay Design 2.0 (version 2.0.1.15) to sequence two target regions. Region 1 sequenced the genomic region chr4:15,780,321-15,780,394 (Human genome build GRCh37/hg19) and contained 13 CpG sites. Primers for region 1 were as follows: forward, 5′–TGGGTATTGAGGGGATA GTAG-3′; reverse (biotinylated), 5′-AACCCCAAACTCCCTACTCAACA-3′; sequencing, 5′-TTGAGGGGATAGTAGGGT-3′. Region 2 sequenced genomic region chr4:15,780,514-15,780,586 and contained 6 CpG sites. Primers for region 2 were as follows: forward (biotinylated), 5′-TGGTGTTGAGTAGGGAGT-3′; reverse, 5′-CCAC AAACTTTACAAACCACTTAAATATCC-3′; sequencing, 5′-AAAATAAACTACAAC-3′. Genomic DNA (1 μg) from each sample ($n = 2$) was treated with sodium bisulfite using the EZ 96-DNA Methylation Kit (Zymo Research), following the manufacturer's standard protocol. Pyrosequencing was performed according to the PyroMark MD protocol and sequenced with a PyroMark Q96 MD instrument. Methylation analysis was performed with Pyro Q-CpG (version 1.0.9).

qRT-PCR gene expression analysis

Prostate cancer cells were seeded in 10-cm dishes and treated with either ATRA (1.2 μmol/L) or azacytidine (5 μmol/L) for 96 hours. LNCaP cells treated with doxycycline (1 μg/mL) for 96 hours served as the positive control. Cells were then harvested, washed twice with PBS, and lysed in Qiagen RLT buffer supplemented with 2-mercaptoethanol (140 μmol/L; Sigma-Aldrich). DNA/RNA purification was performed using an AllPrep DNA/RNA Mini Kit (Qiagen). qPCR was performed using a Roche LightCycler II and 1-Step Brilliant SYBR Green qRT-PCR master mix (Agilent Technologies). Forward and reverse primer sequences for CD38 primer sets 1 and 2 and β-actin were as follows: CD38 forward 1: 5′-CGCGATGCGTCAAGTACACTGAA-3′, CD38 reverse 1: 5′-CGGTCTGAGTTCCCAACTTCATTAG-3′; CD38 forward 2: 5′-GGAGAAAGGACT: GCAGCAACAACC-3′, CD38 reverse 2: 5′-CTGCGGGATCCATTGAGCATCACAT-3′; β-actin forward: 5′-CGG AGT ACT TGC GCT CAG GA-3′, β-actin reverse: 5′-CCA CGA AAC TAC CTT CAA CTC CAT CAT G-3′. The Roche LightCycler 489 protocol was as follows: 50°C for 30 minutes, 95°C for 10 minutes, then a three-step amplification (30 seconds at 95°C, 30 seconds at 55°C, 1 minute at 68°C) × 45 cycles, rest at 4°C. Changes in gene expression were determined using the $\Delta\Delta C_t$ method as described previously (19).

Measurement of extracellular acidification rates and oxygen consumption rates

Prostate cancer cells were pretreated either with vehicle, FK866 (100 nmol/L), FK866 + NMN (500 μmol/L), or FK866 + NAD$^+$ (100 μmol/L) for 24 hours or doxycycline 72 hours prior to plating in 24-well plates and incubated overnight at 37°C (6×10^5 cells/well; XF24 plates, Agilent). To measure extracellular acidification rate (ECAR) and oxygen consumption rate (OCR), RPMI culture medium was changed to minimal DMEM assay media supplemented with glutamine (2 mmol/L; ECAR) or XF Assay Medium supplemented with glucose (25 mmol/L) and sodium pyruvate (1 mmol/L; OCR) followed by a 1-hour incubation at 37°C in the absence of CO_2. Baseline ECAR and OCR were measured on a Seahorse XF24 extracellular flux analyzer (Agilent). Basal glycolytic and mitochondrial functions were established following injections to final concentrations of glucose (10 mmol/L) or oligomycin (1 μmol/L), respectively. Maximum glycolytic and mitochondrial potential were achieved by injecting to a final concentration of oligomycin (1 μmol/L) or carbonyl cyanide 4-(trifluoromethoxy) phenylhydrazone (FCCP; 0.5 μmol/L), respectively. Glycolytic and mitochondrial inhibition were achieved following injection to a final concentration of 2-deoxy-D-glucose (100 mmol/L) or combination of rotenone and antimycin A (1 μmol/L each), respectively. All measurements were normalized to cell counts determined at the conclusion of each assay.

Quantification of glucose and lactate levels

Prostate cancer cells were plated in 6-well plates in triplicate and allowed to adhere overnight prior to treatment with doxycycline (1 μg/mL) for 96 hours. To determine the amount of glucose consumed or lactate produced, the existing culture media were removed, cells were rinsed with PBS, and 1.5 mL of fresh RPMI was added. Samples were taken immediately following media change (T0) and after 12 hours. Glucose and lactate levels were determined using BioVision Glucose and Lactate Assay Kits. Glucose and lactate concentrations were normalized to cellular protein.

Fatty acid and lipid synthesis

Fatty acid and lipid synthesis were determined by incorporation of ^{14}C-acetate or ^{14}C-choline into lipid as described previously (18). Briefly, 5×10^5 cells treated with vehicle or doxycycline (1 μg/mL) for 72 hours were seeded in 24-well plates for 24 hours ($n = 4$ wells/treatment). Cells were incubated with ^{14}C-acetate (1 μCi) or ^{14}C-choline (1 μCi) for 2 hours. Cells were then harvested, washed with PBS, and lysed in hypotonic buffer [20 mmol/L Tris-HCL (pH 7.5), 1 mmol/L EDTA, and 1 mmol/L DTT]. The lipid fraction was extracted using chloroform/methanol (2:1), and incorporation of labeled acetate or choline into newly synthesized lipid was determined by scintillation counting and normalized to cellular protein.

Metabolite profiling

Metabolomic profiling was conducted on PC3 cells treated with vehicle or FK866 (100 nmol/L) for 24 hours ($n = 4$). Samples were collected and submitted for analysis as directed by Metabolon, Inc. Onsite sample preparation was carried out

Downloaded from http://aacrjournals.org/mcr/article-pdf/16/11/1687/2312911/1687.pdf by guest on 27 August 2022

using an automated MicroLab STAR system utilizing a series of proprietary organic and aqueous extractions to remove the protein fraction. Samples were analyzed on gas chromatography/mass spectrometry and LC/MS-MS platforms and analyzed against known libraries of purified compounds as described previously (20). Statistical significance for pair-wise comparisons was determined using Welch *t* tests and/or Wilcoxon rank sum tests. Compound clustering and classification was performed using random forest analyses (21). All statistical modeling was performed using R.

Genomic analysis

RNA sequencing (RNA-Seq) analysis was conducted in the Cancer Genomics Shared Resource of Wake Forest Baptist Comprehensive Cancer Center. LNCaP cells transfected with either an empty vector or CD38 expression construct were plated (5×10^5 cells/dish) in 10-cm dishes and treated with doxycycline (1 μg/mL) for 96 hours ($n = 5$/group). Total RNA was purified from cell lines using the RNeasy Plus Micro Kit (Qiagen) with genomic DNA removal. RNA integrity (RIN) was assessed via electrophoretic tracing on an Agilent Bioanalyzer. RNA-Seq libraries were constructed from samples (RIN > 7.0) using an Illumina TruSeq Stranded Total RNA Kit with Ribo-Zero Gold rRNA depletion. Libraries were sequenced on an Illumina NextSeq 500 DNA sequencer using 75-nt single-end reads generating 45 to 55 million uniquely mapped reads/sample. The quality of raw sequencing reads was evaluated by FASTQC analysis (Babraham Bioinformatics). Read alignment was conducted using the STAR sequence aligner and gene counts established using Feature Counts software (22, 23). Differentially expressed genes (DEG) were verified using the DESeq2 algorithm, and statistically significant results were defined as $P \leq 0.05$ after adjusting for false discovery (Benjamini–Hochberg; ref. 24).

Gene set enrichment analysis was performed as described by Subramanian and colleagues (25). Briefly, genes with base mean values below five reads were eliminated from analysis, and $\log_2$ fold changes were arranged in descending order. Gene symbols were loaded into GSEA software and run against hallmark gene symbol v6.0 with a false collapsable dataset run at 1,000 permutations.

CD38 gene expression and methylation status were investigated using The Cancer Genome Atlas (TCGA) prostate adenocarcinoma (PRAD) provisional dataset ($n = 491$) as accessed through the cBioPortal Web Resource (26). Methylation (HM450) β-values for *CD38* were plotted against *CD38* RNA-Seq (V2 RSEM) expression values using the cBioPortal query interface (http://www.cbioportal.org/). Pearson and Spearman correlations were used to evaluate the relationship between the two measures.

Survival analysis of SLC22A3 expression as a predictor of biochemical recurrence was performed using GraphPad Prism version 5.00 for Windows. Survival and expression data were derived from patient samples from two independent cohorts (27, 28). SLC22A3-low expression was defined as values one SD below the mean relative to the remainder (SLC22A3-high). Statistical significance was derived using log-rank (Mantel–Cox) analysis.

Statistical analysis

Data were graphically displayed using bar charts or boxplots to allow groups to be compared visually. Pairwise comparisons were made using unpaired two-tailed *t* tests. Groups were compared using one-way ANOVA models. If there was evidence of an overall difference among groups (i.e., significant F-test in ANOVA), subsequent pairwise comparisons were made using multiple comparison adjustments Tukey HSD (honest significant difference) as appropriate to determine which groups differed from each other. For gene expression analysis, a linear contrast was fit in the ANOVA model to examine whether there was a linear relationship in the outcome going across the groups ordered benign, PIN, prostate cancer, and Met-HR. Levels of significance were denoted by three groupings: *, $P \leq 0.05$; **, $P \leq 0.01$; and ***, $P \leq 0.001$; comparisons with *P* values between 0.01 and 0.05 were considered as marginally significant to account for multiple comparisons being made, whereas *P* values less than 0.01 were considered as statistically significant accounting for multiple comparisons.

Results

CD38 expression is inversely correlated with prostate cancer progression

In order to understand the role of CD38 in prostate cancer, protein expression was first determined in PRECs and the tumorigenic C4-2, PC3, LNCaP, and DU145 cell lines. PRECs expressed CD38, whereas expression was nearly absent in the tumorigenic lines (Fig. 1A). Consistent with CD38 expression and its reported NADase activity, PRECs had lower total NAD^+ levels compared with tumorigenic lines with 2.5 nmol/μg protein, whereas the tumorigenic lines ranged from 5.23 to 11.8 nmol/μg protein ($P \leq 0.05$; Fig. 1A). It has been demonstrated that low CD38 expression is associated with both biochemical recurrence and metastasis (16). The GEO dataset GSE6099 was used to determine whether *CD38* expression is decreased with prostate cancer progression (29). ANOVA suggested a highly significant group effect between benign, PIN, prostate cancer, and metastatic hormone-refractory (Met-HR) disease states ($F = 23.5$, $P \leq 0.001$; Fig. 1B). Pairwise comparisons revealed benign samples had significantly higher *CD38* expression relative to each of the other stages ($P \leq 0.001$). Furthermore, expression of *CD38* in PIN margins was greater relative to both prostate cancer ($P \leq 0.05$) and Met-HR ($P \leq 0.019$). There was no difference between prostate cancer and Met-HR. Linear contrast analysis (1 degree of freedom) of the trend in expression across all four groups was found to be highly significant ($F = 54.33$, $P \leq 0.001$; Fig. 1B). CD38 protein expression was also determined by IHC. ANOVA followed by *post hoc* Student–Newman–Keuls analysis demonstrated a 24% reduction of CD38 staining intensity in benign versus PIN, 36% decrease in PIN versus prostate cancer, and a 50% decrease in benign versus prostate cancer ($P \leq 0.001$, Fig. 1C). Overall these results indicate loss of CD38 expression during prostate cancer progression occurs in a stepwise manner and is correlated with elevated NAD^+ levels.

Expression of CD38 reduces total NAD^+ levels and inhibits cell proliferation

To determine whether CD38 acts as an NADase in prostate cancer, total NAD^+ levels were determined following CD38 induction. Induction of CD38 in DU145, LNCaP, and PC3 cells was confirmed by Western blot analysis and was sufficient to reduce total NAD^+ levels in DU145 cells by 31%, in LNCaP cells

Downloaded from http://aacrjournals.org/mcr/article-pdf/16/11/1687/2312911/1687.pdf by guest on 27 August 2022

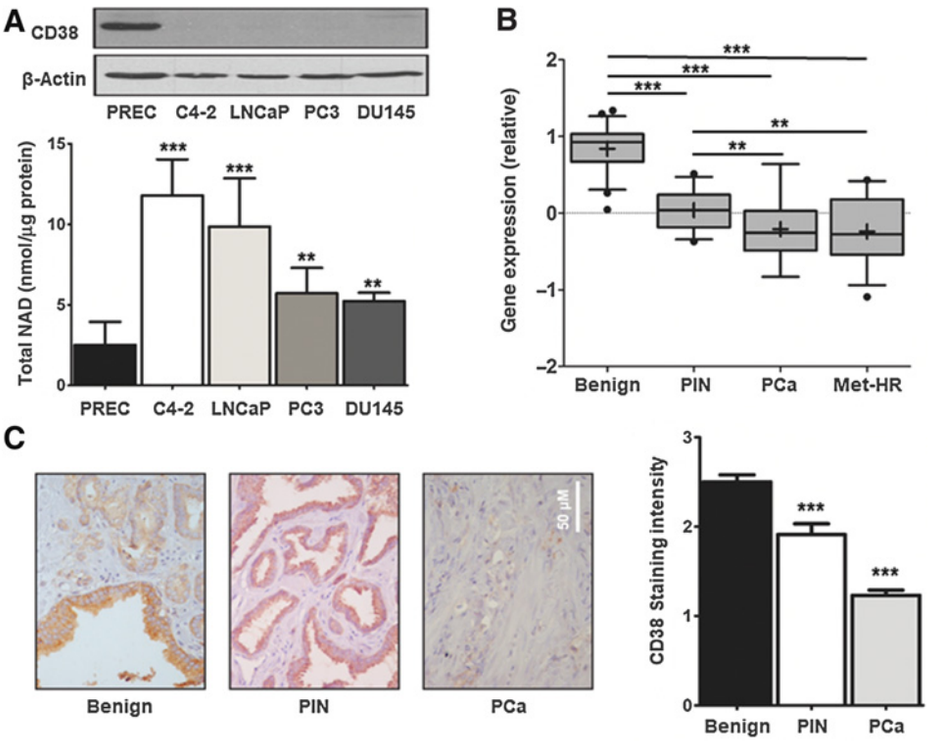

Figure 1.
CD38 expression is inversely correlated with prostate cancer progression. **A,** CD38 protein expression was determined by Western blot analysis in PREC and prostate cancer (PCa) cells. Colorimetric determination of total NAD^+ levels in PREC and prostate cancer cell lines ($n = 3$). **B,** Quantification of relative *CD38* expression from patient samples in GEO database GSE6099 containing benign ($n = 22$), PIN ($n = 13$), prostate cancer ($n = 29$), and Met-HR ($n = 17$) samples (29). **C,** CD38 expression was determined by IHC on a tissue microarray containing benign ($n = 37$), PIN ($n = 17$), and prostate cancer ($n = 37$). Staining intensity was independently scored on a scale of 0 to 3 (*, $P \leq 0.05$; **, $P \leq 0.01$; ***, $P \leq 0.001$).

by 29%, and in PC3 cells by 91% relative to vehicle ($P \leq 0.05$; Fig. 2A). DU145 empty vector cells treated with doxycycline showed no significant change in total NAD^+ (Fig. 2A). These data support the notion that CD38 can alter NAD^+ levels between normal and cancer cells. Sirtuins require NAD^+ for their catalytic activity and FOXO1 is one SIRT1 substrate whose activity is regulated by acetylation and affected by changes in NAD^+ levels (30). Therefore, we next determined the impact of CD38 on FOXO1 acetylation. Expression of CD38 increased FOXO1 acetylation 3.4-fold, similar to what was observed following treatment with sirtinol (Fig. 2B) or the NAMPT inhibitor FK866 (Fig. 2B). The effect on acetylation was independent of CD38-induced change in Sirt1 and 3 expression (Fig. 2C). The impact of CD38 expression on cell proliferation was determined by trypan blue exclusion in all three cell lines. CD38 induced a significant proliferation blockade at multiple time points with the most significant effects occurring in DU145 (34%, $P \leq 0.01$), LNCaP (32%, $P \leq 0.001$), and PC3 (21%, $P \leq 0.001$) cells at 96 hours postinduction, without increasing dead cells. This demonstrates that CD38 is sufficient to inhibit proliferation by limiting NAD^+ (Fig. 2D, G, and J). Decreased cell numbers were accompanied by a small but significant G_0–G_1 blockade and subsequent reduction of cells in S and G_2–M (Fig. 2E, H, and K). Moreover, CD38 expression increased the doubling time of DU145 cells from 44 to 55.6 hours, of LNCaP cells from 36 to 44.5 hours, and of PC3 cells from 44 to 59.8 hours ($P < 0.01$; Fig. 2F, I, and L). Although CD38 reduced proliferation, cells expressing CD38 remained sensitive to NAMPT inhibition by FK866, as has been previously demonstrated in pancreatic cancer (17). Treatment of CD38-expressing cells with 2.5, 5, and 10 nmol/L FK866 further reduced viability by 17%, 36%, and 39%, respectively ($P \leq 0.01$; Fig. 2M). These data reveal the requirement for NAD^+ by prostate cancer cells.

CD38 expression is induced by ATRA

There is a retinoic acid response element (RARE) in the *CD38* promoter and RA can induce CD38 expression in some cells (31, 32). Prostate cancer cells were treated with ATRA to see whether CD38 expression can be induced and overcome silencing. Treatment with ATRA was sufficient to induce expression of CD38 in three prostate cancer cell lines, although there was no dose effect over the range tested (Fig. 3A). ATRA also reduced total NAD^+ in LNCaP and DU145 cells ($P \leq 0.01$), which correlated with a significant decrease in cell number ($P \leq 0.01$, Fig. 3B and C). These data provide another demonstration of the connection between CD38 and NAD^+ in prostate cancer. The presences of CpG islands spanning exon 1 and intron 1 of the *CD38* gene can be methylated (33, 34). TCGA PRAD provisional dataset also demonstrated that there is a significant inverse correlation between *CD38* expression and *CD38* methylation (Pearson $R = -0.667$, Spearman $= -0.826$), suggesting that *CD38* may be subject to negative regulation by methylation in prostate cancer (Fig. 3D). LNCaP and PC3 cells were treated with ATRA and azacytidine to determine their impact on the methylation status of 19 potential methylation sites (Fig. 3E and G). Although there is some difference in the overall methylation status of *CD38* among these sites, ATRA did not impact the methylation status of either site, despite significant *CD38* expression in LNCaP and PC-3 cells ($P \leq 0.001$; Fig. 3F and H). On the other hand, azacytidine reduced the overall methylation of *CD38* in PC3 ($P \leq 0.05$) but not LNCaP cells while increasing *CD38* expression in both cell lines ($P \leq 0.001$; Fig. 3F and H). These data suggest that ATRA can induce CD38 expression, although not through changes in the CpG sites analyzed here. They also suggest that methylation is a mechanism that contributes to decreased CD38 expression in prostate cancer.

Downloaded from http://aacrjournals.org/mcr/article-pdf/16/11/1687/2312911/1687.pdf by guest on 27 August 2022

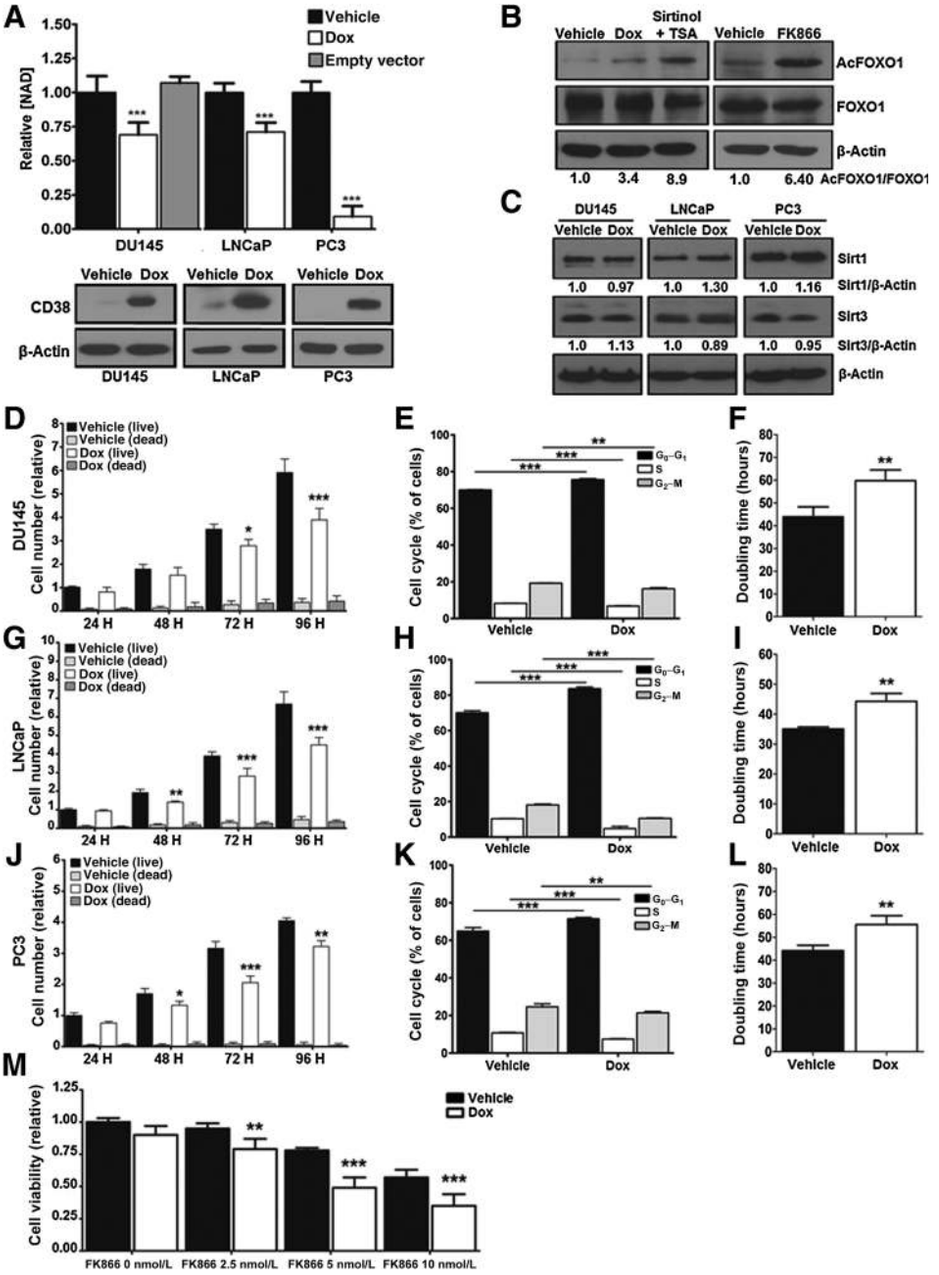

Figure 2.

CD38 reduces total NAD^+ and inhibits cell proliferation. **A,** Total NAD^+ levels were measured in prostate cancer cells following treatment with vehicle (dH_2O) or doxycycline (1 μg/mL) for 96 hours ($n = 3$). Expression of CD38 and β-actin in prostate cancer cells determined by Western blot analysis following 96-hour treatment with doxycycline (1 μg/mL). **B,** Expression of acetylated-FOXO1, total FOXO1, and β-actin in PC3 cells determined by Western blot analysis in response to CD38 expression or treatment with FK866 (100 nmol/L). Treatment with sirtinol (100 μmol/L) and trichostatin A (500 μmol/L) for 18 hours served as positive control. The ratio of acetylated/total FOXO1 was determined by densitometry of single bands using β-actin as a loading control. **C,** Expression of Sirt1, Sirt3, and β-actin in prostate cancer cells was determined by Western blot analysis following 96-hour treatment with doxycycline (1 μg/mL). Changes in Sirt1 or Sirt3 expression were determined by densitometry of single bands using β-actin as a loading control. **D, G,** and **J,** Relative cell counts of live and dead prostate cancer cells determined by trypan blue exclusion of cells treated with doxycycline (1 μg/mL) for the indicated times ($n = 3$). **E, H,** and **K,** Cell-cycle analysis of prostate cancer cells treated with doxycycline (1 μg/mL) for 96 hours. Signal intensity of incorporated propidium iodide corresponding to DNA content was used to gate cells into G_0–G_1, S, and G_2–M phases ($n = 3$). **F, I,** and **L,** Doubling time of prostate cancer cells from following 96-hour treatment with doxycycline (1 μg/mL; $n = 3$). **M,** Viability of DU145 cells treated with doxycycline (1 μg/mL) for 72 hours followed by 24-hour treatment with FK866 at the indicated concentration ($n = 3$; *, $P \leq 0.05$; **, $P \leq 0.01$; ***, $P \leq 0.001$).

CD38 reduces glycolytic and mitochondrial capacity

The role of CD38 in regulating cellular metabolism was determined at several levels. The effect of CD38 on glycolysis was determined by Seahorse analysis. Figure 4A illustrates the influence of CD38 on the ECAR of DU145 cells. Quantification of the ECAR demonstrates that CD38 reduced basal glycolysis and glycolytic capacity by 32% and 44%, respectively ($P \leq 0.05$; Fig. 4B). Similarly, CD38 in PC3 cells reduced basal glycolysis by 27% and glycolytic capacity by 30% ($P \leq 0.05$; Fig. 4C). CD38 did not affect either basal glycolysis or glycolytic capacity in LNCaP cells (Fig. 3D). Mitochondrial stress assays were performed to determine the effect of CD38 expression on cellular OCRs. Figure 4E illustrates the influence of CD38 on the OCR of LNCaP cells. When quantified, basal respiration was reduced by 24% ($P \leq 0.05$), maximal respiration by 45% ($P \leq 0.01$), and spare respiratory capacity by 25% ($P \leq 0.05$; Fig. 4F). In PC3 cells, CD38 reduced basal respiration by 43% ($P \leq 0.001$), maximal respiration by 39% ($P \leq 0.01$), and spare respiratory capacity by 27% ($P \leq 0.05$; Fig. 4G). In DU145 cells, CD38 reduced basal OCR by 36% ($P \leq 0.05$), maximal respiration by 39% ($P \leq 0.05$), and spare respiratory capacity by 35% ($P \leq 0.05$; Fig. 4H). In accordance with decreased ECAR, CD38 reduced glucose consumption from 14.3 to 7.1 μmol/L/μg protein and 15.2 to 8.1 μmol/L/μg protein in DU145 and PC3 cells, respectively ($P \leq 0.001$; Fig. 4I and J). A concomitant decrease in lactate production

Downloaded from http://aacrjournals.org/mcr/article-pdf/16/11/1687/2312911/1687.pdf by guest on 27 August 2022

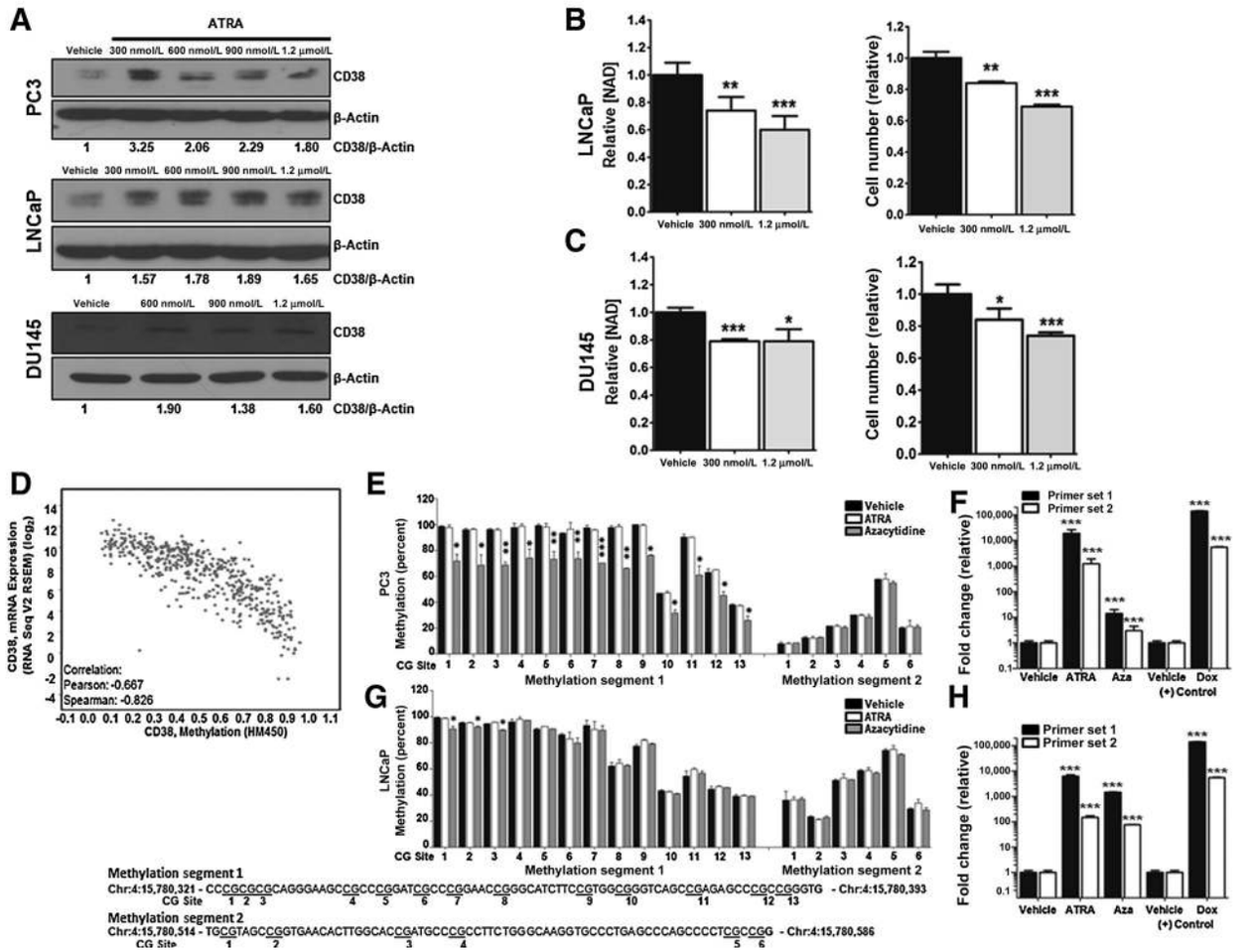

Figure 3.

CD38 expression is induced by ATRA. **A,** Expression of CD38 following 96-hour treatment with ATRA at the indicated concentration. **B** and **C,** NAD^+ levels and cell counts in LNCaP and DU145 cells treated for with ATRA for 96 hours ($n = 3$). **D,** *CD38* expression as a function of methylation status determined using data from the TCGA prostate adenocarcinoma (PRAD) provisional data set ($n = 491$). **E** and **G,** Pyrosequencing data from PC3 and LNCaP cells representing the percent of methylated CG sites in two segments of intron 1 of the *CD38* gene following 96-hour treatment with ATRA (1.2 μmol/L) or azacytidine (5 μmol/L; $n = 2$). **F** and **H,** Fold change in CD38 mRNA in response to treatment with ATRA (1.2 μmol/L) or azacytidine (5 μmol/L) for 96 hours (*, $P \leq 0.05$; **, $P \leq 0.01$; ***, $P \leq 0.001$).

from 23.2 to 18.4 μmol/L/μg protein in DU145 cells ($P \leq 0.001$) and 25.3 to 16 μmol/L/μg protein in PC3 cells ($P < 0.001$) accompanied decreased glucose consumption (Fig. 4I and J). These data provide novel insight into metabolic regulation by CD38 and suggest *CD38* silencing is required for full metabolic capacity in prostate cancer cells.

Pharmacologic inhibition of NAMPT reduces glycolytic and mitochondrial capacity

Because CD38 expression may mimic inhibition of NAD^+ synthesis, the metabolic consequences of NAMPT inhibition were determined. Figure 5A illustrates the impact of NAMPT inhibition by FK866 on the ECAR of PC3 cells. NAMPT inhibition reduced basal glycolysis and glycolytic capacity by 30% and 49%, respectively ($P \leq 0.001$; Fig. 5B), both of which were fully restored with exogenous NMN or NAD^+. Similar results were observed in DU145 cells where basal glycolysis was reduced by 29% ($P \leq 0.05$) and glycolytic capacity by 40% ($P \leq 0.05$; Fig. 5C). Similar to the effects of CD38 on ECAR, there were no observed differences in LNCaP cells following NAMPT inhibition (Fig. 5D). We next determined the consequence of NAMPT inhibition on OCR in PC3 cells (Fig. 5E). Maximal respiration and spare respiratory capacity were reduced by 37% ($P \leq 0.01$) and 35% ($P \leq 0.01$), respectively (Fig. 5F). Supplementation of NMN and NAD^+ rescued the effect of FK866. DU145 cells had a more pronounced reduction in maximal respiration and spare respiratory capacity, being reduced by 54% ($P \leq 0.01$) and 56% ($P \leq 0.01$), respectively (Fig. 5G). No changes in either measurement were detected in LNCaP cells (Fig. 5H).

To complement glycolytic and mitochondrial flux assays, metabolite levels were measured following NAMPT inhibition in PC3 cells (Fig. 5I–K). As expected, treatment with FK866 reduced the NAD^+ metabolites nicotinamide, NAD^+, NADH,

Downloaded from http://aacrjournals.org/mcr/article-pdf/16/11/1687/2312911/1687.pdf by guest on 27 August 2022

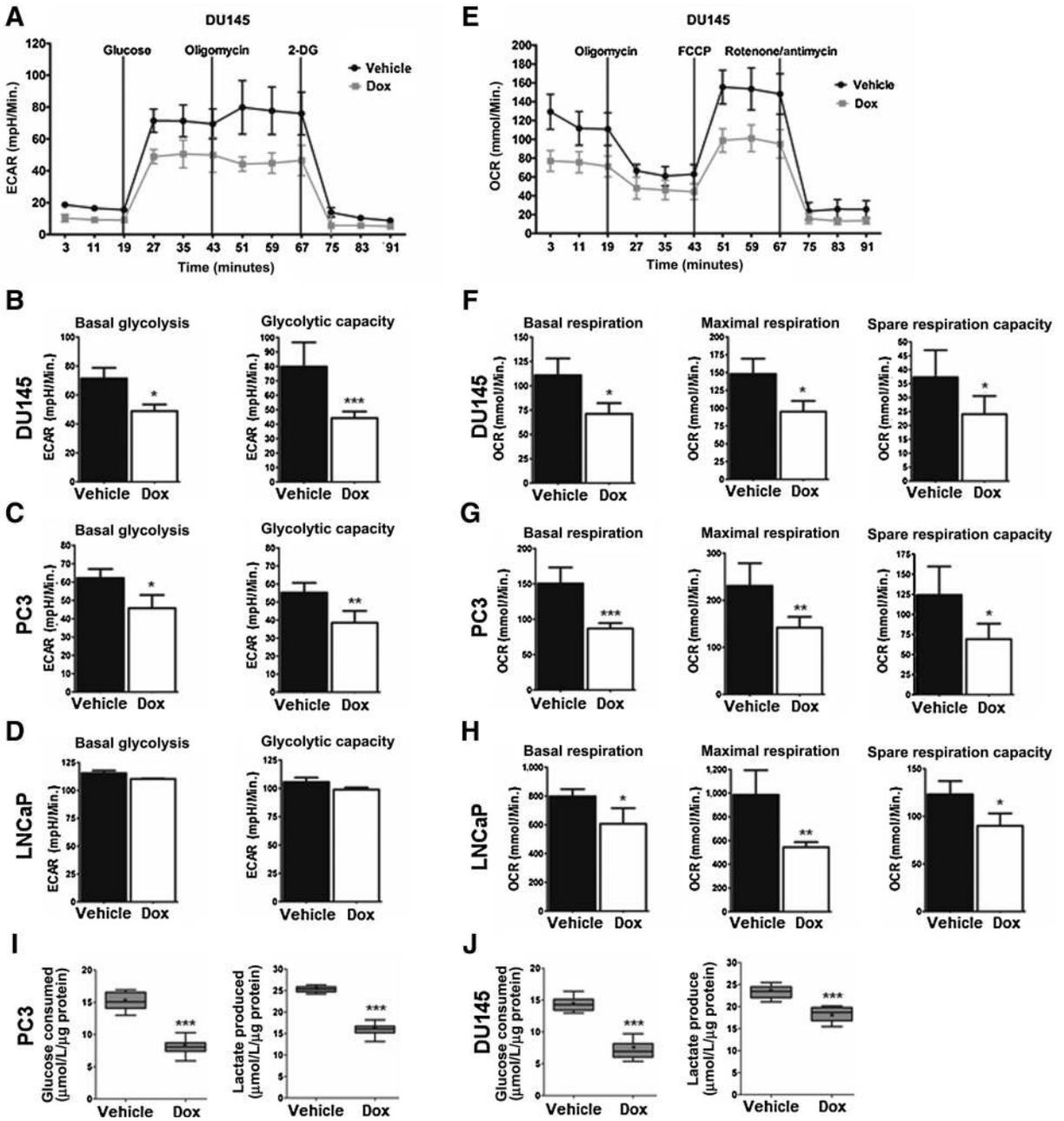

Figure 4.

CD38 reduces glycolytic and mitochondrial capacity. **A,** Representative trace of a glycolytic stress test in DU145 cells following treatment with doxycycline (1 µg/mL) for 96 hours to induce CD38 ($n = 3$). **B–D,** Quantification of basal glycolysis and glycolytic capacity in DU145, PC3, and LNCaP cells treated with doxycycline (1 µg/mL) for 96 hours ($n = 3$). **E,** Representative trace of a mitochondrial stress test in DU145 cells following treatment with doxycycline (1 µg/mL) for 96 hours ($n = 3$). **F–H,** Quantification of basal respiration, maximal respiration, and spare respiratory capacity in DU145, PC3, and LNCaP cells treated with vehicle (dH_2O) or doxycycline (1 µg/mL) for 96 hours ($n = 3$). **I–J,** Quantification of glucose consumed or lactate produced in PC3 and DU145 cells following 96-hour treatment with doxycycline (1 µg/mL; $n = 6$; *, $P \leq 0.05$; **, $P \leq 0.01$; ***, $P \leq 0.001$).

and $NADP^+$ by 87%, 86%, 71%, and 95% relative to vehicle, respectively ($P \leq 0.001$; Fig. 5I). Metabolites involved in glycolysis upstream of GAPDH, the reaction in glycolysis that utilizes NAD^+ as a cofactor, were increased. Specifically, glucose, glucose-6-phosphate, and sorbitol were increased by 56%, 91%, and 35% relative to vehicle, respectively ($P \leq 0.05$; Fig. 5J). Lactate, the byproduct of glycolysis, was decreased by 14% ($P \leq 0.05$; Fig. 5J). Metabolites in the TCA cycle, which contains multiple enzymes that utilize NAD^+ as a cofactor, were also affected. Citrate and succinate were reduced to 77% ($P \leq 0.05$) and 36% ($P \leq 0.001$)

Downloaded from http://aacrjournals.org/mcr/article-pdf/16/11/1687/2312911/1687.pdf by guest on 27 August 2022

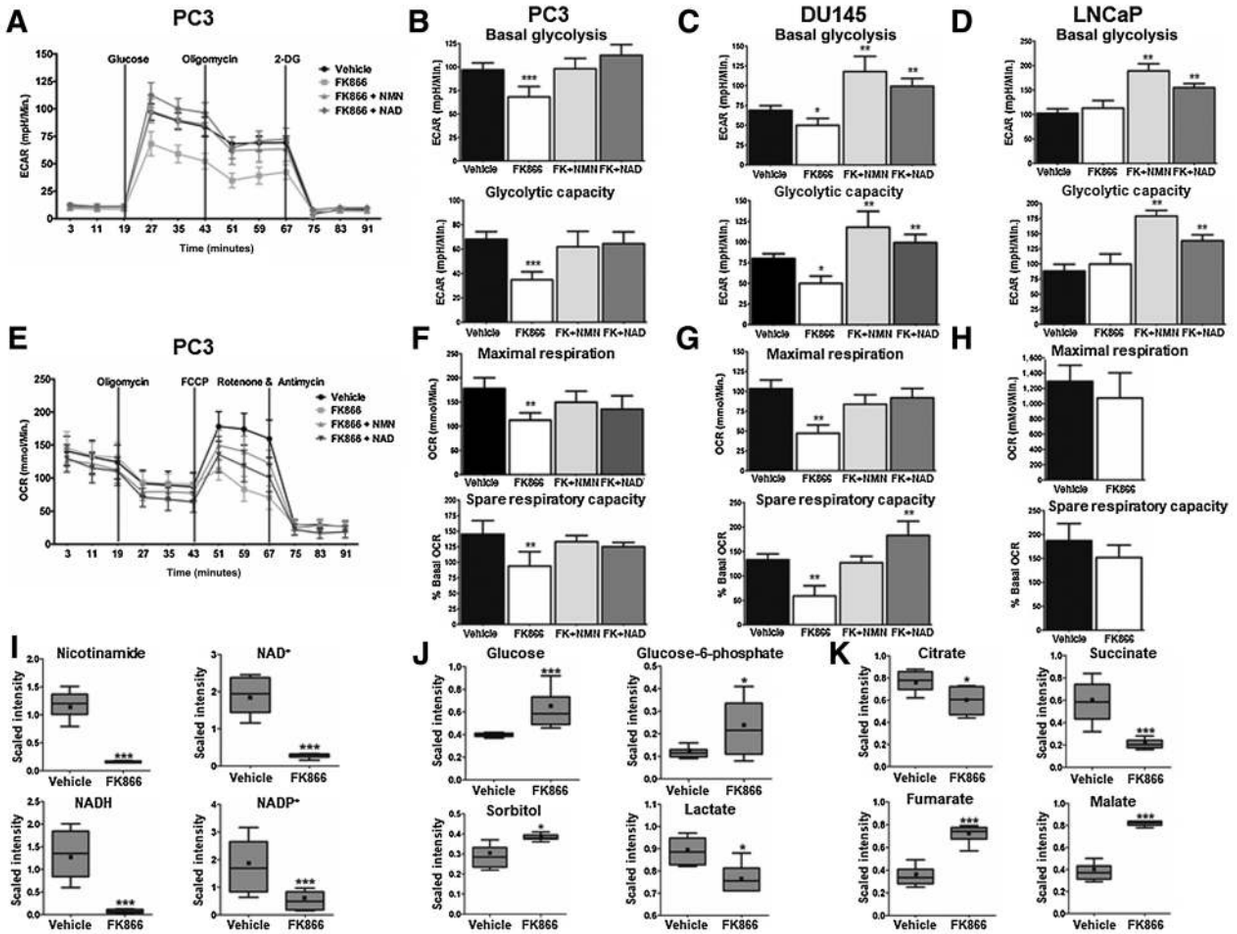

Figure 5.

Pharmacologic inhibition of NAMPT reduces glycolytic and mitochondrial capacity. **A,** Representative trace of a glycolytic stress test in PC3 cells following treatment with FK866 (100 nmol/L) for 24 hours in the absence or presence of exogenous NMN (500 μmol/L) or NAD$^+$ (100 μmol/L; $n = 3$). **B–D,** Quantification of basal glycolysis and glycolytic capacity in DU145, PC3, and LNCaP cells ($n = 3$). **E,** Representative trace mitochondrial stress test in PC3 cells following treatment with FK866 (100 nmol/L) for 24 hours in the absence or presence of exogenous NMN (500 μmol/L) or NAD$^+$ (100 μmol/L; $n = 3$). **F–H,** Quantification of basal respiration, maximal respiration, and spare respiratory capacity in PC3, DU145, and LNCaP cells ($n = 3$). **I–K,** Scaled intensity of nicotinamide containing metabolites (**I**), glycolytic metabolites (**J**), and TCA cycle metabolites (**K**) following treatment of PC3 cells with FK866 (100 nmol/L) for 24 hours (*, $P \leq 0.05$; **, $P \leq 0.01$; ***, $P \leq 0.001$).

of vehicle (Fig. 5K). Fumarate and malate, metabolites upstream of malate dehydrogenase, an NAD$^+$-dependent enzyme, were increased 207% ($P \leq 0.001$) and 218% ($P \leq 0.001$) relative to vehicle (Fig. 5K). These data directly align with the effects of CD38 on glycolytic and mitochondrial metabolism, providing additional evidence to the importance of NAD$^+$ balance, and that CD38 expression closely mimics NAMPT inhibition.

Expression of CD38 activates AMPK and inhibits fatty acid and lipid synthesis

We previously reported that NAMPT inhibition activates AMPK and subsequently inactivates acetyl-CoA carboxylase 1 (ACC1), resulting in decreased fatty acid and lipid synthesis (18). Similarly, CD38 increased the pAMPK/AMPK ratio in PC3, DU145, and LNCaP cells by 1.86-fold, 3.95-fold, and 1.79-fold, respectively (Fig. 6A). Consistent with AMPK activation, the ratio of pACC to total ACC in PC3, DU145, and LNCaP cells increased by 2.39-fold, 10.85-fold, and 1.94-fold, respectively. There was little change in FASN levels (Fig. 6A). In line with inactivation of ACC1, incorporation of ^{14}C-acetate into fatty acid was reduced by 34% in PC3 cells, 20% in DU145 cells, and by 48% in LNCaP cells ($P \leq 0.01$, Fig. 6B). Expression of CD38 had similar effects on the incorporation of ^{14}C-choline into the lipid fraction. Lipid synthesis was reduced by 35%, 32%, and 26% in PC3, DU145, and LNCaP cells, respectively ($P \leq 0.01$; Fig. 6C). Taken together, these results indicate that CD38 impedes energy production and substrate flow, resulting in activation of AMPK and the subsequent inhibition of fatty acid and lipid synthesis.

CD38 reprograms the transcriptome of prostate cancer cells

To better understand the global impact of CD38 on LNCaP cells, RNA-Seq was used to determine the extent to which it altered gene expression and biological processes. Of the

Downloaded from http://aacrjournals.org/mcr/article-pdf/16/11/1687/2312911/1687.pdf by guest on 27 August 2022

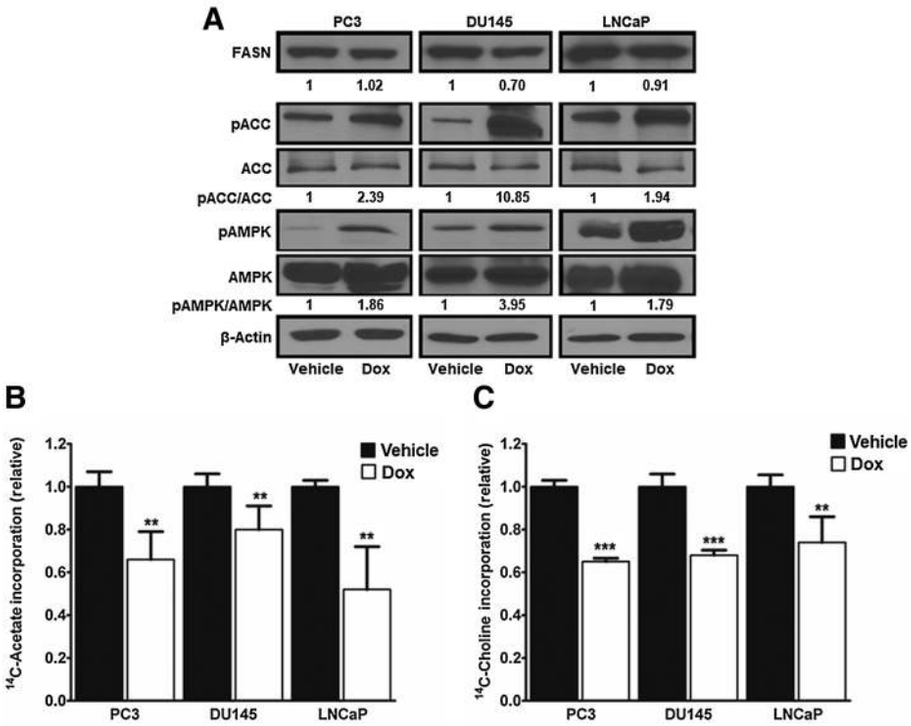

Figure 6.
Expression of CD38 activates AMPK and inhibits fatty acid and lipid synthesis. **A,** FASN, phospho-ACC, ACC, phospho-AMPK, AMPK, and β-actin levels determined by Western blot analysis in PC3, DU145, and LNCaP cells following induction of CD38 by doxycycline (1 μg/mL). Phospho-to-total ratios were determined by densitometry of single bands using β-actin as a loading control. **B,** Fatty acid synthesis in PC3, DU145, and LNCaP cells as determined by incorporation of ^{14}C-acetate into lipid following induction of CD38 for 96 hours ($n = 3$). **C,** Lipid synthesis in PC3, DU145, and LNCaP cells as determined by incorporation of ^{14}C-choline into lipid following induction of CD38 for 96 hours ($n = 3$; *, $P \leq 0.05$; **, $P \leq 0.01$; ***, $P \leq 0.001$).

34,000 genes analyzed, 14,409 (41%) genes had significant differential expression following induction of CD38 ($P \leq 0.05$, FDR-adjusted). The data were further gated to include only transcripts with a $\log_2$ fold change of $1 \leq x \leq -1$, revealing 1,082 (3.1%) upregulated and 828 (2.4%) downregulated genes (data not shown). Gene set enrichment analysis was performed to define molecular signatures consistent with the RNA-Seq expression profile (Fig. 7A–C). Consistent with the effects of CD38 on proliferation, multiple pathways associated with reduced proliferation were affected by CD38 expression. Among them, the E2F targets (Q-value ≤ 0.0001) were the most significant (Fig. 7A). As an example, *CDKN1A* expression was increased 2.85-fold by CD38 expression, consistent with a nonproliferative phenotype. Similar to what has been reported in pancreatic cancer, CD38 expression caused an increase in $p21^{Cip1}$ protein expression of 1.53-fold, 6.0-fold, and 1.96-fold in PC3, DU145, and LNCaP cells, respectively, following CD38 expression. Other pathways, including Notch signaling (Q-value $= 0.005$), and G_2–M checkpoint (Q-value ≤ 0.0001), were also highly correlated as signatures that exhibited decreased expression following induction of CD38 (Fig. 7B and C). As each pathway carries an important role in cell proliferation, these data establish a connection between expression of CD38 and a reprogramming of the transcriptome in favor of a nonproliferative phenotype. Although the metabolic consequences of CD38 expression in prostate cancer were broad, it appears that the effects are primarily attributed to changes in cellular NAD^+ and not decreases in metabolic gene expression. In general, the relative gene expression levels of enzymes involved in glycolysis, the TCA cycle, fatty acid synthesis, and the electron transport chain were below the 2-fold cutoff despite multiple transcripts achieving statistical significance (Table 1). It is important to note that of the glycolytic enzymes, there was no change in *GAPDH*, the only enzyme in glycolysis that requires NAD^+. Similarly, expression levels of genes encoding TCA cycle enzymes were similarly unaltered, with the greatest changes occurring in pyruvate dehydrogenase kinase (*PDK1*; 1.49-fold), aconitase 1 (*ACO2*; 1.5-fold), and isocitrate dehydrogenase 1 (*IDH1*; 1.5-fold). These data provide further evidence that decreased mitochondrial output is not the result of decreased gene expression but rather limited availability of NAD^+ to facilitate enzymatic activity. The single greatest change of any metabolic gene occurred in *FASN*, which was reduced 1.92-fold ($P \leq 0.0001$, FDR-adjusted), although there was no detectable change in protein levels. In addition to gene set enrichment analysis, the most differentially expressed gene in the dataset was selected for analysis. *SLC22A3* expression increased more than 300-fold (Fig. 7D). SLC22A3 protein expression was also increased in LNCaP cells following induction of CD38 and NAMPT inhibition (Fig. 7D). Interestingly, the SNP rs936455 in *SLC22A3* is the single most highly correlated SNP with prostate cancer (35). *SLC22A3* is also one of the most significantly downregulated genes in high Gleason grade tumors (29). Therefore, the correlation between biochemical recurrence and *SLC22A3* expression was determined in the Taylor and Yu cohorts, which contain 181 primary and 37 metastases or 66 primary and 83 normal (adjacent or donor) samples, respectively (27, 28). Consistent with the inverse association between *SLC22A3* and high Gleason grade tumors, high *SLC22A3* was associated with increased time to biochemical recurrence in the Taylor and Yu cohorts (Fig. 7E). These data establish a novel connection between CD38 and cellular processes, aside from metabolism, that regulates proliferation and is associated with prostate cancer progression.

Downloaded from http://aacrjournals.org/mcr/article-pdf/16/11/1687/2312911/1687.pdf by guest on 27 August 2022

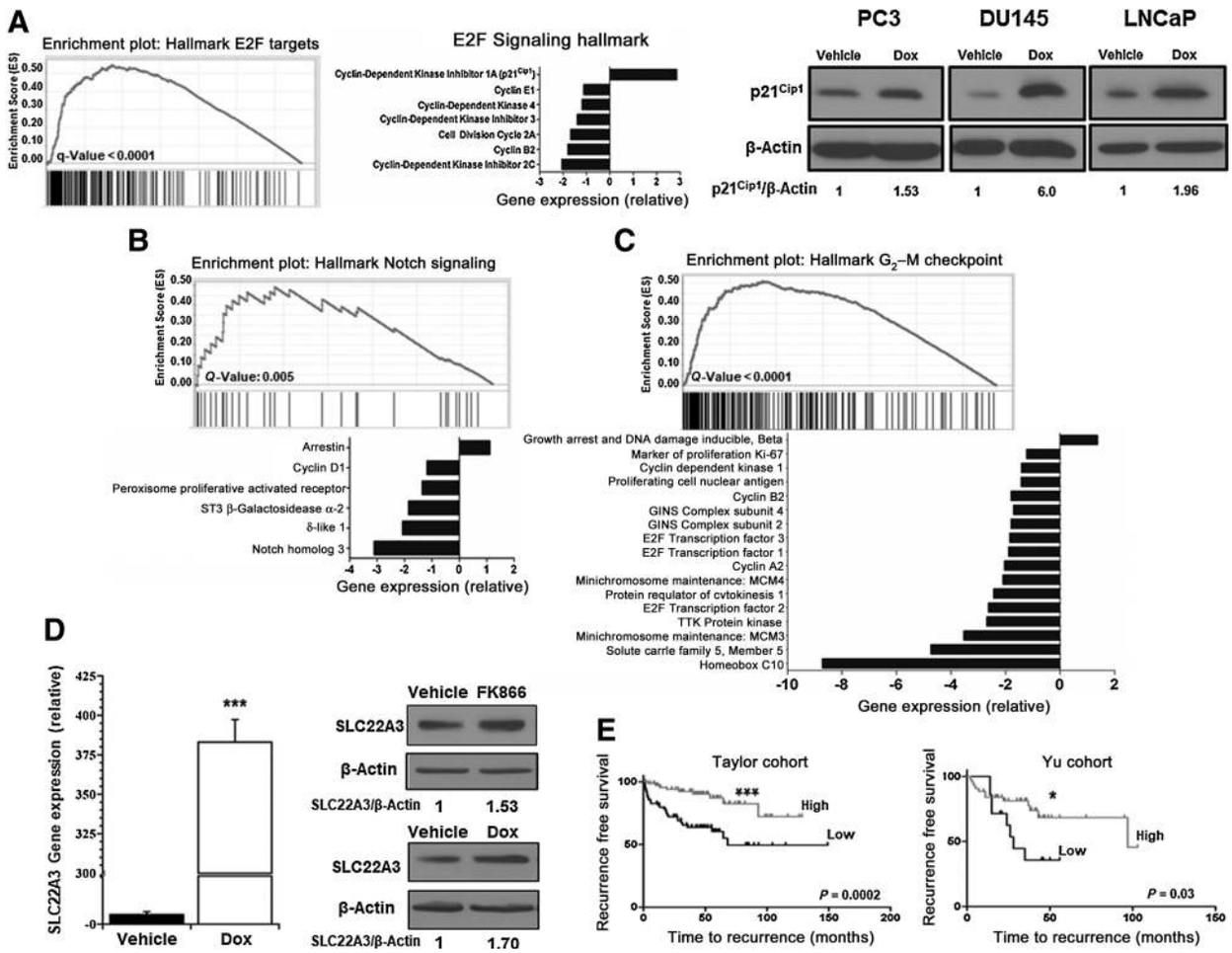

Figure 7.

CD38 reprograms the transcriptome of prostate cancer cells. **A,** Gene set enrichment plot of genes altered by CD38 also included in an established E2F target hallmark signature (M5925). The bar graph represents gene expression values for a subset of genes contained in the E2F hallmark gene list. Expression of the cell-cycle inhibitor p21^{Cip1} was determined by Western blotting following treatment with doxycycline (1 μg/mL) for 96 hours with β-actin as a loading control. **B,** Gene set enrichment plot of the genes affected by CD38 within a hallmark NOTCH signaling gene set (M5903). The bar graph represents relative expression levels of a subset of genes within the NOTCH signaling hallmark indicative of a nonproliferative phenotype. **C,** Gene set enrichment plot of genes affected by CD38 that exhibit a similar expression pattern to genes contained within the hallmark G_2–M checkpoint (M6901). The bar graph represents relative expression of genes contained within the G_2–M checkpoint hallmark consistent with a nonproliferative phenotype. **D,** *SLC22A3* expression in LNCaP cells following induction of CD38. Expression of SLC22A3 in LNCaP cells determined by Western blot analysis following treatment with FK866 (100 nmol/L) for 24 hours or doxycycline (1 μg/mL) for 96 hours, respectively. **E,** Recurrence-free survival as a function of SLC22A3 in the Taylor and Yu cohorts (*, $P \leq 0.05$; **, $P \leq 0.01$; ***, $P \leq 0.001$; refs. 27, 28).

Discussion

Tumor cells require an available pool of NAD$^+$ for appropriate metabolic control and posttranslational protein modification, among other functions, to support survival and proliferation. Intracellular NAD$^+$ levels can be modulated by increased synthesis, in particular through the salvage pathway, where NAMPT is the rate-limiting enzyme. In fact, NAMPT expression is increased in several cancers, partially illustrating the importance of NAD$^+$ in tumor biology (36). One of the principal roles of NAD$^+$ is as a cofactor in metabolic reactions, serving to support hydride transfer reactions. Although these reactions affect whether NAD$^+$ is oxidized or reduced, they do not consume or alter NAD$^+$ levels. CD38 is the primary NADase in mammalian cells (10). Here, we demonstrate that CD38 expression is decreased in prostate cancer and regulates the metabolic potential of prostate cancer cells. This provides a mechanistic explanation for why loss of CD38 in prostate luminal progenitor cells results in prostate cancer, particularly in response to inflammation (16).

Although we and others have demonstrated that CD38 expression is reduced in prostate cancer, the mechanism by which CD38 expression is decreased is unknown. The *CD38* gene is located on chromosome 4p15.32; a region not frequently lost in prostate cancer (37). Using the TCGA PRAD provisional dataset, we establish a strong negative correlation between *CD38* methylation and expression. This suggests that epigenetics could be a determinant of CD38 expression in prostate cancer. Interestingly,

Downloaded from http://aacrjournals.org/mcr/article-pdf/16/11/1687/2312911/1687.pdf by guest on 27 August 2022

Table 1. CD38 does not alter metabolic pathway gene expression

Pathway	Gene symbol	Gene name	Fold change	P_{adj}
Glycolysis	HK1	Hexokinase 1	1.59 ± 0.12	0.0000
	HK2	Hexokinase 2	1.26 ± 0.04	0.0000
	GCK	Glucokinase (hexokinase 4)	1.14 ± 0.55	0.6570
	GPI	Glucose-6-phosphate isomerase	1.03 ± 0.06	0.1792
	GAPDH	Glyceraldehyde-3-phosphate dehydrogenase	−1.02 ± 0.07	0.5036
	GLYCTK	Glycerate kinase	−1.16 ± 0.07	0.0043
	ENO1	Enolase 1, (alpha)	−1.09 ± 0.05	0.0000
	PKM	Pyruvate kinase, muscle	−1.48 ± 0.05	0.0000
	LDHA	Lactate dehydrogenase A	1.14 ± 0.05	0.0000
	LDHB	Lactate dehydrogenase B	1.14 ± 0.06	0.0000
Tricarboxylic acid cycle	PDK1	Pyruvate dehydrogenase kinase, isozyme 1	1.49 ± 0.04	0.0000
	CS	Citrate synthase	1.18 ± 0.07	0.0000
	ACO1	Aconitase 1, soluble	−1.27 ±0.05	0.0000
	ACO2	Aconitase 2, mitochondrial	1.50 ± 0.10	0.0000
	IDH1	Isocitrate dehydrogenase 1 ($NADP^+$), soluble	1.50 ± 0.09	0.0000
	IDH2	Isocitrate dehydrogenase 2 ($NADP^+$), mitochondrial	−1.29 ± 0.06	0.0000
	OGDH	Oxoglutarate (alpha-ketoglutarate) dehydrogenase	−1.14 ± 0.11	0.0000
	MDH1	Malate dehydrogenase 1, NAD (soluble)	1.14 ± 0.05	0.0000
	MDH2	Malate dehydrogenase 2, NAD (mitochondrial)	1.11 ± —	0.0000
	PC	Pyruvate carboxylase	1.04 ± 0.06	0.1195
Fatty acid synthesis	ACLY	ATP citrate lyase	1.11 ± 0.06	0.0000
	ACACA	Acetyl-CoA carboxylase; alpha	−1.17 ± 0.04	0.3451
	ACACB	Acetyl-CoA carboxylase; beta	1.24 ± 0.15	0.0000
	FASN	Fatty acid synthase	−1.92 ± 0.03	0.0000
NADH dehydrogenase (complex I)	NDUFA1	NADH dehydrogenase (ubiquinone) 1; α subcomplex 1	1.22 ± 0.12	0.0000
	NDUFA5	NADH dehydrogenase (ubiquinone) 1; α subcomplex 5	1.04 ± 0.04	0.1617
	NDUFA6	NADH dehydrogenase (ubiquinone) 1; α subcomplex 6	1.35 ± 0.07	0.0000
	NDUFA7	NADH dehydrogenase (ubiquinone) 1; α subcomplex 7	1.12 ± 0.07	0.0000
	NDUFA9	NADH dehydrogenase (ubiquinone) 1; α subcomplex 9	1.31 ± 0.09	0.0000
	NDUFA12	NADH dehydrogenase (ubiquinone) 1; α subcomplex 12	1.18 ± 0.09	0.0000
Succinate dehydrogenase (complex II)	SDHA	Succinate dehydrogenase complex (subunit A)	1.28 ± 0.08	0.0000
	SDHB	Succinate dehydrogenase complex (subunit B)	1.22 ± 0.07	0.0000
	SDHC	Succinate dehydrogenase complex (subunit C)	−1.11 ± 0.07	0.0008
	SDHD	Succinate dehydrogenase complex (subunit D)	1.09 ± 0.04	0.0003
Cytochrome C reductase (complex III)	UQCRB	Ubiquinol-cytochrome c reductase; binding protein	1.22 ± 0.09	0.0000
	UQCRC1	Ubiquinol-cytochrome c reductase; core protein I	1.01 ± 0.09	0.7548
	UQCRC2	Ubiquinol-cytochrome c reductase; core protein II	1.19 ± 0.06	0.0000
	UQCR10	Ubiquinol-cytochrome c reductase; complex III (subunit X)	1.47 ± 0.11	0.0000
	UQCR11	Ubiquinol-cytochrome c reductase; complex III (subunit XI)	1.09 ± 0.09	0.0000
Cytochrome C oxidase (complex IV)	COX10	COX10 heme A:farnesyltransferase cytochrome c oxidase assembly factor	1.10 ± 0.08	0.0071
	COX14	COX14 cytochrome c oxidase assembly factor	1.15 ± 0.11	0.0000
ATP synthase (F_O complex)	ATP5F1	ATP synthase; mitochondrial Fo complex (subunit B1)	1.13 ± 0.07	0.0000
	ATP5S	ATP synthase; mitochondrial Fo complex (subunit S)	−1.06 ± 0.08	0.0989
	ATP5I	ATP synthase; mitochondrial Fo complex (subunit E)	1.01 ± 0.09	0.6758
	ATP5L	ATP synthase; mitochondrial Fo complex (subunit G)	1.19 ± 0.09	0.0000
ATP synthase (F_1 complex)	ATPAF1	ATP synthase mitochondrial F1 complex; assembly factor 1	1.08 ± 0.06	0.0000
	ATPAF2	ATP synthase mitochondrial F1 complex; assembly factor 2	−1.03 ± 0.08	0.3633

NOTE: Metabolic pathway gene expression as a function of CD38. Fold changes are expressed relative to vehicle control ± SD ($n = 5$).

CD38 has CpG islands that span exon 1 and intron 1 that may be potential epigenetic regulatory sites (34). Moreover, *CD38* also has a RARE in its promoter region (33). The data demonstrate that ATRA is sufficient to induce CD38 expression, but not through the CpG sites tested. Similarly, azacytidine can induce CD38 expression, although likely through other CpG sites as well because expression in LNCaP was independent of changes in the examined sites. Overall, the data suggest that strategies to induce CD38 expression could be one mechanism to decrease NAD^+ in prostate cancer and perhaps affect therapeutic response and hint that there are epigenetic or other elements in *CD38* that regulate its expression.

The data also demonstrate a direct link between CD38 and metabolic capacity in prostate cancer. Expression of CD38 reduced the glycolytic and mitochondrial potential of prostate cancer cell lines reflected by decreases in ECAR and OCR. This is in line with decreased NAD^+ levels and reduced proliferation. Interestingly, decreased CD38 expression in prostate cancer is opposite of that in aging where CD38 expression increases with age (38). On the other hand, in both cases, CD38 regulates mitochondrial metabolism. It is worth noting that, although CD38 reduced the OCR in LNCaP cells, there was no observed effect on ECAR. Moreover, LNCaP cells rely less on glycolysis and more on mitochondrial metabolism, so the metabolic impact of CD38 is most likely primarily through mitochondrial metabolism. These findings are in line with previous reports, including ours, that some cells are resistant to NAMPT inhibition; perhaps indicating that NAD^+ can exist in distinct pools

Downloaded from http://aacrjournals.org/mcr/article-pdf/16/11/1687/2312911/1687.pdf by guest on 27 August 2022

in some cells (18, 39, 40). Thus, we posit that CD38 targets mitochondrial NAD^+ pools in all lines tested. It appears that most of the metabolic consequences of CD38 expression are due to diminished total NAD^+ rather than changes in expression as the majority of metabolic enzymes showed no change at the mRNA level following CD38 expression. However, it does not rule out the enzymes being affected by acetylation as CD38 induces acetylation of the Sirt1 substrate FOXO1 and also affects the acetylation status of p53 (41). Because sirtuins can regulate metabolic processes including ATP production, antioxidative stress response, lipid synthesis, and the metabolic switch to anaerobic glycolysis (42, 43), we posit that CD38 impacts cellular metabolism through acetylation and depleted metabolite flow by limiting available NAD^+.

Prostate cancer has a lipogenic phenotype indicated by high expression of lipogenic enzymes and increased uptake of metabolic tracers of lipogenesis (44). We previously reported the link between NAD^+ synthesis and lipogenesis in prostate cancer (18). In line with this, CD38 expression induced AMPK activation and subsequent phosphorylation of the canonical AMPK substrate ACC1. Accordingly, CD38 reduced fatty acid and lipid synthesis, suggesting that reduced CD38 expression is required in some part to support the lipogenic phenotype associated with prostate cancer. Interestingly, CD38 does not have a significant impact on ACC1 or FASN expression, suggesting that CD38 regulates bioenergetics and substrate flow through the pathway, but that oncogenic drivers control enzyme expression. It is noteworthy that CD38 expression in prostate cancer mimics the metabolic consequences of NAMPT inhibition, as assessed by OCR, ECAR, and lipid synthesis, suggesting that alterations in NAD^+ levels, regardless of the cause, yield similar results.

Although CD38 clearly affects cellular metabolism, it also impacts pathways that control proliferation, including Notch signaling, E2F targets, and G_2–M checkpoint. Notch signaling has both pro- and antiproliferative potential in prostate cancer and is linked to metastatic disease (45, 46). Interestingly, Notch signaling can be triggered by Sirt1 activation and modulated in response to variations in NAMPT expression (47). Additionally, activated NOTCH is a known repressor of $p21^{Cip1}$ expression in prostate cancer (48). Therefore, it is reasonable that CD38 expression suppressed NOTCH signaling and increased $p21^{Cip1}$ expression in the E2F signaling hallmark. In addition to indicators of reduced proliferation, CD38 also affects *SLC22A3* expression. Decreased SLC22A3 expression is associated with tumor progression and poor patient survival in a variety of solid tumors including ovarian, pancreatic, and prostate cancer (49, 50). Moreover, *SLC22A3* is among the most downregulated genes in high Gleason grade prostate cancer (29, 51). Our data demonstrate a correlation between SLC22A3 and recurrence-free survival, and the same is also true for CD38 (16), suggesting a correlation between the two genes in prostate cancer. Silencing of *SLC22A3* in prostate is regulated by genetic polymorphisms in the proximal promoter and aberrant methylation of the promoter region (52). In prostate cancer cell lines, the *SLC22A3* promoter is variably methylated, with LNCaP cells being less methylated than in DU145 and PC3 cells (52). This may explain why CD38 and FK866 induce SLC22A3 in LNCaP cells but not PC3 and DU145 cells. These data provide the first demonstration that changes in NAD^+ metabolism can regulate SLC22A3.

Collectively, the data illustrate a novel connection between CD38, modulation of NAD^+, and prostate cancer tumor cell metabolism. We propose a model in which silencing of CD38 elevates NAD^+ bioavailability and reprograms prostate cells in favor of macromolecule biosynthesis and a pro-proliferative phenotype. The finding that low CD38 expression in luminal progenitor cells is sufficient to initiate prostate cancer (16), combined with our metabolic and gene expression data, provides a critical connection between CD38, NAD^+ metabolism, and prostate cancer progression.

Disclosure of Potential Conflicts of Interest

No potential conflicts of interest were disclosed.

Authors' Contributions

Conception and design: J.P. Chmielewski, S.D. Cramer, S.J. Kridel
Development of methodology: J.P. Chmielewski, G. Sui, S.D. Cramer, S.J. Kridel
Acquisition of data (provided animals, acquired and managed patients, provided facilities, etc.): J.P. Chmielewski, F.B. Wheeler, L. Shi, A.L. Davis, T.D. Howard, S.J. Sirintrapun, S.D. Cramer, S.J. Kridel
Analysis and interpretation of data (e.g., statistical analysis, biostatistics, computational analysis): J.P. Chmielewski, L. Shi, T.D. Howard, R.B. D'Agostino Jr, L.D. Miller, S.D. Cramer, S.J. Kridel
Writing, review, and/or revision of the manuscript: J.P. Chmielewski, F.B. Wheeler, R.B. D'Agostino Jr, L.D. Miller, S.J. Sirintrapun, S.D. Cramer, S.J. Kridel
Administrative, technical, or material support (i.e., reporting or organizing data, constructing databases): J.P. Chmielewski, S.C. Bowlby
Study supervision: J.P. Chmielewski

Acknowledgments

This research was supported by 5R01CA16503 (S.J. Kridel) and 5T32Hl091797-10 (J.P. Chmielewski). Research reported in this publication was supported by the NCI's Cancer Center Support Grant award number P30CA012197 issued to the Wake Forest Baptist Comprehensive Cancer Center. The content is solely the responsibility of the authors and does not necessarily represent the official views of the NCI.

The costs of publication of this article were defrayed in part by the payment of page charges. This article must therefore be hereby marked *advertisement* in accordance with 18 U.S.C. Section 1734 solely to indicate this fact.

Received September 21, 2017; revised June 1, 2018; accepted July 13, 2018; published first August 3, 2018.

References

1. Chiarugi A, Dolle C, Felici R, Ziegler M. The NAD metabolome–a key determinant of cancer cell biology. Nat Rev Cancer 2012;12:741–52.
2. Verdin E. NAD(+) in aging, metabolism, and neurodegeneration. Science 2015;350:1208–13.
3. Di Stefano M, Conforti L. Diversification of NAD biological role: the importance of location. FEBS J 2013;280:4711–28.
4. Hanahan D, Weinberg RA. Hallmarks of cancer: the next generation. Cell 2011;144:646–74.
5. Kennedy BE, Sharif T, Martell E, Dai C, Kim Y, Lee PW, et al. NAD(+) salvage pathway in cancer metabolism and therapy. Pharmacol Res 2016;114:274–83.
6. Hasmann M, Schemainda I. FK866, a highly specific noncompetitive inhibitor of nicotinamide phosphoribosyltransferase, represents a novel

Downloaded from http://aacrjournals.org/mcr/article-pdf/16/11/1687/2312911/1687.pdf by guest on 27 August 2022

mechanism for induction of tumor cell apoptosis. Cancer Res 2003;63: 7436–42.
7. Li XL, Kazgan N. Mammalian sirtuins and energy metabolism. Int J Biol Sci 2011;7:575–87.
8. Jagtap P, Szabo C. Poly(ADP-ribose) polymerase and the therapeutic effects of its inhibitors. Nat Rev Drug Discov 2005;4:421–40.
9. Lee HC. Structure and enzymatic functions of human CD38. Mol Med 2006;12:317–23.
10. Aksoy P, White TA, Thompson M, Chini EN. Regulation of intracellular levels of NAD: A novel role for CD38. Biochem Biophys Res Commun 2006;345:1386–92.
11. Shrimp JH, Hu J, Dong M, Wang BS, MacDonald R, Jiang H, et al. Revealing CD38 cellular localization using a cell permeable, mechanism-based fluorescent small-molecule probe. J Am Chem Soc 2014;136:5656–63.
12. Liang M, Chini EN, Cheng J, Dousa TP. Synthesis of NAADP and cADPR in mitochondria. Arch Biochem Biophys 1999;371:317–25.
13. Kramer G, Steiner G, Fodinger D, Fiebiger E, Rappersberger C, Binder S, et al. High expression of a CD38-like molecule in normal prostatic epithelium and its differential loss in benign and malignant disease. J Urol 1995;154:1636–41.
14. Liu AY, Roudier MP, True LD. Heterogeneity in primary and metastatic prostate cancer as defined by cell surface CD profile. Am J Pathol 2004;165: 1543–56.
15. Zhao YJ, Graeff R, Lee HC. Roles of cADPR and NAADP in pancreatic cells. Acta Biochim Biophys Sin 2012;44:719–29.
16. Liu X, Grogan TR, Hieronymus H, Hashimoto T, Mottahedeh J, Cheng DH, et al. Low CD38 identifies progenitor-like inflammation-associated luminal cells that can initiate human prostate cancer and predict poor outcome. Cell Rep 2016;17:2596–606.
17. Chini CC, Guerrico AM, Nin V, Camacho-Pereira J, Escande C, Barbosa MT, et al. Targeting of NAD metabolism in pancreatic cancer cells: potential novel therapy for pancreatic tumors. Clin Cancer Res 2014;20:120–30.
18. Bowlby SC, Thomas MJ, D'Agostino RB, Kridel SJ. Nicotinamide phosphoribosyl transferase (Nampt) is required for de novo lipogenesis in tumor cells. PLoS One 2012;7:e40195.
19. Schmittgen TD, Livak KJ. Analyzing real-time PCR data by the comparative C-T method. Nat Protoc 2008;3:1101–8.
20. DeHaven CD, Evans AM, Dai HP, Lawton KA. Organization of GC/MS and LC/MS metabolomics data into chemical libraries. J Cheminform 2010;2:9.
21. Breiman L. Random forests. Machine Learning 2001;45:5–32.
22. Dobin A, Davis CA, Schlesinger F, Drenkow J, Zaleski C, Jha S, et al. STAR: ultra fast universal RNA-seq aligner. Bioinformatics 2012;29:15–21.
23. Liao Y, Smyth G, Shi W. featureCounts: an efficient general purpose progarm for assigning sequence rease to genomic features. Bioinformatics 30–30:923;2014.
24. Love M, Huber W, Anders S. Moderated estimation of fold change and dispersion for RNA-seq data with DESeq2. Genome Biol 2014;12:550.
25. Subramanian A, Tamayo P, Mootha VK, Mukherjee S, Ebert BL, Gillette MA, et al. Gene set enrichment analysis: a knowledge-based approach for interpreting genome-wide expression profiles. Proc Natl Acad Sci USA 2005;102:15545–50.
26. Gao J, Aksoy BA, Dogrusoz U, Dresdner G, Gross B, Sumer SO, et al. Integrative analysis of complex cancer genomics and clinical profiles using the cBioPortal. Sci Signal 2013;6:pl1.
27. Taylor BS, Schultz N, Hieronymus H, Gopalan A, Xiao Y, Carver BS, et al. Integrative genomic profiling of human prostate cancer. Cancer Cell 2010; 18:11–22.
28. Yu YP, Landsittel D, Jing L, Nelson J, Ren B, Liu L, et al. Gene expression alterations in prostate cancer predicting tumor aggression and preceding development of malignancy. J Clin Oncol 2004;22:2790–9.
29. Tomlins SA, Mehra R, Rhodes DR, Cao X, Wang L, Dhanasekaran SM, et al. Integrative molecular concept modleing of prostate cancer progression. Nat Genet 2016;49:41–51.
30. Liu HY, Xing R, Cheng XF, Li QR, Liu F, Ye H, et al. De-novo NAD(+) synthesis regulates SIRT1-FOXO1 apoptotic pathway in response to NQO1 substrates in lung cancer cells. Oncotarget 2016;7:62503–19.
31. Kishimoto H, Hoshino S, Ohori M, Kontani K, Nishina H, Suzawa M, et al. Molecular mechanism of human CD38 gene expression by retinoic acid - identification of retinoic acid response element in the first intron. J Biol Chem 1998;273:15429–34.
32. Uruno A, Noguchi N, Matsuda K, Nata K, Yoshikawa T, Chikamatsu Y, et al. All-trans retinoic acid and a novel synthetic retinoid tamibarotene (Am80) differentially regulate CD38 expression in human leukemia HL-60 cells: possible involvement of protein kinase C-δ. J Leukoc Biol 2011;90:235–47.
33. Ferrero E, Saccucci F, Malavasi F. The human CD38 gene: polymorphism, CpG island, and linkage to the CD157 (BST-1) gene. Immunogenetics 1999;49:597–604.
34. Nata K, Takamura T, Karasawa T, Kumagai T, Hashioka W, Tohgo A, et al. Human gene encoding CD38 (ADP-ribosyl cyclase/cyclic ADP-ribose hydrolase): Organization, nucleotide sequence and alternative splicing. Gene 1997;186:285–92.
35. Eeles RA, Kote-Jarai Z, Giles GG, Al Olama AA, Guy M, Jugurnauth SK, et al. Multiple newly identified loci associated with prostate cancer susceptibility. Nat Genet 2008;40:316–21.
36. Garten A, Petzold S, Korner A, Imai S, Kiess W. Nampt: linking NAD biology, metabolism and cancer. Trends Endocrinol Metab 2009;20: 130–8.
37. Robinson D, Van Allen Eliezer M, Wu YM, Schultz N, Lonigro Robert J, Mosquera JM, et al. Integrative clinical genomics of advanced prostate cancer. Cell 2015;161:1215–28.
38. Camacho-Pereira J, Tarrago MG, Chini CCS, Nin V, Escande C, Warner GM, et al. CD38 dictates age-related NAD decline and mitochondrial dysfunction through an SIRT3-dependent mechanism. Cell Metab 2016;23:1127–39.
39. Tolstikov V, Nikolayev A, Dong S, Zhao G, Kuo MS. Metabolomics analysis of metabolic effects of nicotinamide phosphoribosyltransferase (NAMPT) inhibition on human cancer cells. PLoS One 2014;9:e114019.
40. Stein LR, Imai S. The dynamic regulation of NAD metabolism in mitochondria. Trends Endocrinol Metab 2012;23:420–8.
41. Aksoy P, Escande C, White TA, Thompson M, Soares S, Benech JC, et al. Regulation of SIRT 1 mediated NAD dependent deacetylation: a novel role for the multifunctional enzyme CD38. Biochem Biophys Res Commun 2006;349:353–9.
42. Haigis MC, Sinclair DA. Mammalian sirtuins: biological insights and disease relevance. Annu Rev Pathol 2010;5:253–95.
43. Hallows WC, Lee S, Denu JM. Sirtuins deacetylate and activate mammalian acetyl-CoA synthetases. Proc Natl Acad Sci U S A 2006;103:10230–5.
44. Liu QP, Luo Q, Halim A, Song GB. Targeting lipid metabolism of cancer cells: a promising therapeutic strategy for cancer. Cancer Lett 2017; 401:39–45.
45. Su Q, Xin L. Notch signaling in prostate cancer: refining a therapeutic opportunity. Histol Histopathol 2016;31:149–57.
46. Bin Hafeez B, Adhami VM, Asim M, Siddiqui IA, Bhat KM, Zhong W, et al. Targeted knockdown of Notch1 inhibits invasion of human prostate cancer cells concomitant with inhibition of matrix metalloproteinase-9 and urokinase plasminogen activator. Clin Cancer Res 2009;15:452–9.
47. Wang P, Du H, Zhou CC, Song J, Liu X, Cao X, et al. Intracellular NAMPT-NAD+-SIRT1 cascade improves post-ischaemic vascular repair by modulating Notch signalling in endothelial progenitors. Cardiovasc Res 2014; 104:477–88.
48. Lefort K, Ostano GP, Mello-Grand M, Calpini V, Scatolini M, Farsetti A, et al. Dual tumor suppressing and promoting function of Notch1 signaling in human prostate cancer. Oncotarget 2016;7:48011–26.
49. Mohelnikova-Duchonova B, Strouhal O, Hughes DJ, Holcatova I, Oliverius M, Kala Z, et al. SLC22A3 polymorphisms do not modify pancreatic cancer risk, but may influence overall patient survival. Sci Rep 2017;7:43812.
50. Heise M, Lautem A, Knapstein J, Schattenberg JM, Hoppe-Lotichius M, Foltys D, et al. Downregulation of organic cation transporters OCT1 (SLC22A1) and OCT3 (SLC22A3) in human hepatocellular carcinoma and their prognostic significance. BMC Cancer 2012;12:109.
51. True L, Coleman I, Hawley S, Huang CY, Gifford D, Coleman R, et al. A molecular correlate to the Gleason grading system for prostate adenocarcinoma. Proc Natl Acad Sci U S A 2006;103:10991–6.
52. Chen L, Hong C, Chen EC, Yee SW, Xu L, Almof EU, et al. Genetic and epigenetic regulation of the organic cation transporter 3, SLC22A3. Pharmacogenomics J 2013;13:110–20.

Downloaded from http://aacrjournals.org/mcr/article-pdf/16/11/1687/2312911/1687.pdf by guest on 27 August 2022